

Session 3P6

Novel Mathematical Methods

Far-field RCS Prediction from Measured Near-field Data over Ground Plane	
<i>Y. Inasawa (Mitsubishi Electric Corporation, Japan); S. Kuroda (Mitsubishi Electric Corporation, Japan); S. Morita (Mitsubishi Electric Corporation, Japan); H. Nishikawa (Mitsubishi Electric Corporation, Japan); N. Yoneda (Mitsubishi Electric Corporation, Japan); S. Makino (Mitsubishi Electric Corporation, Japan);</i>	958
Estimation of Buried Pipes Diameter and Position by Ground Penetrating Radar Scans	
<i>G. Borgioli (Universitàdi Firenze, Italy); P. Falorni (Universitàdi Firenze, Italy); L. Capineri (Universitàdi Firenze, Italy); B. Morini (Universitàdi Firenze, Italy); S. Matucci (Universitàdi Firenze, Italy); C. G. Windsor (116, New Road, East Hagbourne, OX11 9LD, UK);</i>	959
The Parallelization of a 2D Floating Random-walk Algorithm for the Solution of the Nonlinear Poisson-boltzmann Equation	
<i>K. Chatterjee (Massachusetts Institute of Technology, USA); J. Poggie (Wright-Patterson Air Force Base, USA);</i>	960
Reduction of FDTD Simulation Time with Modal Methods	
<i>D. A. Gorodetsky (University of Cincinnati, USA); P. A. Wilsey (University of Cincinnati, USA);</i>	961
Approximate Decomposition for the Solution of Boundary Value Problems for Elliptic Systems Arising in Mathematical Models of Layered Structures	
<i>Y. Shestopalov (Karlstad University, Sweden); N. Kotik (Karlstad University, Sweden);</i>	965
Generation of Diverse Time-series Data though Monitoring a Death-multiple Immigration Population Model	
<i>J. O. Matthews (University of Nottingham, UK); K. I. Hopcraft (University of Nottingham, UK); E. Jake-man (University of Nottingham, UK);</i>	970
Implementation of the PML in the CIP Method	
<i>Y. Ando (The University of Electro-Communications, Japan); M. Hayakawa (The University of Electro-communications, Japan);</i>	971
Some Elliptic Traveling Wave Solutions to the Novikov-Veselov Equation	
<i>J. Nickel (University of Osnabruck, Germany); V. S. Serov (University of Oulu, Finland); H. W. Schurmann (University of Osnabruck, Germany);</i>	972
Source Representations of the Debye Potentials in Spherical Coordinates	
<i>M. J. Lahart (U.S. Army Research Laboratory, USA);</i>	977
On the Stability of the Electromagnetic Field in Inhomogeneous Anisotropic Media With Dispersion	
<i>N. V. Budko (Delft University of Technology, The Netherlands); A. B. Samokhin (Moscow University of Radioengineering and Electronics, Russia);</i>	978
Scattering of Electromagnetic Waves by Inhomogeneous Dielectric Gratings Loaded with Perfectly Conducting Strips	
<i>T. Yamasaki (Nihon University, Japan); T. Ujiie (Nihon University, Japan); T. Hinata (Nihon University, Japan);</i>	979
Effects of the Resonant Scattering of Intensive Fields by Weakly Nonlinear Dielectric Layer	
<i>V. V. Yatsyk (Nat. Acad. of Sci. of Ukraine, Ukraine);</i>	980
Theoretical Analysis of Convergence of Rao-Wilton-Glisson Method and Subhierarchal Parallel Algorithm for Solving Electric Field Integral Equation	
<i>Y. G. Smirnov (Penza State University, Russia);</i>	984

Far-field RCS Prediction from Measured Near-field Data over Ground Plane

Y. Inasawa, S. Kuroda, S. Morita, H. Nishikawa, N. Yoneda, and S. Makino
Mitsubishi Electric Corporation, Japan

The far-field Radar Cross Section (RCS) measurement of the actual target requires a long measurement range, which can be realized in the outdoor site. One of the problems in outdoor measurement is the difficulty to avoid the effect of ground bounce because the difference between direct and ground-reflected path length is very small. Some measurement sites realize the outdoor RCS measurement in a few kilometer range by the exploitation of the ground bounce. The shorter measurement range may be preferable especially in Japan.

In this paper we evaluate the far-field RCS prediction technique from near-field RCS data measured over the ground plane in order to find out the possibility of the measurement range reduction. We present the results of the far-field RCS prediction from near-field data including the ground bounce. The near-field data is measured on the metal ground plane in an anechoic chamber, not on the actual ground plane because the fundamental characteristics of ground bounce would be evident. The predicted far-field RCS agrees well with the computed far-field RCS for the measurement model with large dimension in horizontal direction. Whereas the small prediction error for the measurement model with large vertical dimension is observed. The applicable scope of the far-field RCS prediction technique over the ground plane is resolved.

Estimation of Buried Pipes Diameter and Position by Ground Penetrating Radar Scans

G. Borgioli, P. Falorni, L. Capineri, B. Morini, and S. Matucci
Università di Firenze, Italy

C. G. Windsor
116, New Road, East Hagbourne, OX11 9LD, UK

The interest of this study is concerned to the problem of determining the position and size of buried pipes by using remote sensing methods like ultra-wide-band radar, which can measure the round trip time (time of flight ToF) of a pulsed wave by an antenna placed just above the surface (y_i). In this study we consider the physical approximation that the diffracted field from the pipe can be received over a wide angle range of antenna positions and so the time of flight information can be measured for several incident field angles. It is common to find in practice pipes that are buried at about one meter under a road with size that is comparable to few radar wavelengths and for them the simple point like scatterer approximation for the time of flight equation doesn't approximate well the experimental data. The aim of this work is to study the feasibility of robust solving methods for the hyperbolic equation of the time of flight, which contains in the most general case four unknown: pipe radius (R), position (lateral y_0 , depth z_0), and propagation velocity (v). A mathematical solution of the system of non linear equations is presented. The derived solution has the advantage to be linear for the solution of a new set of unknown ($\psi = Rv$, $\sigma = v^2$ and y_0). Only the solution for z_0 remains non linear. From the numerical point of view the solution of the linear system is straightforward and the sensitivity to measurements errors superimposed to y_i and ToF has been carried out. The application of the solving method to simulated data for defined values of sampling time and noise has shown the difficulties of accurate estimation of pipes diameter while the lateral position y_0 and velocity have been well approximated by the centroid of the distribution of the solutions. Numerical methods for solving this problem are discussed and data are presented on simulated and experimental data. The accurate estimation of the four unknowns together is important not only for devising advanced non destructive testing methods but also for providing information about the soil velocity distribution that can be exploited by inversion methods in the time domain (linear SAR).

The Parallelization of a 2D Floating Random-walk Algorithm for the Solution of the Nonlinear Poisson-boltzmann Equation

K. Chatterjee

Massachusetts Institute of Technology, USA

J. Poggie

Wright-Patterson Air Force Base, USA

This paper presents the parallelization of a two-dimensional floating random walk (FRW) algorithm for the solution of the nonlinear Poisson-Boltzmann (NPB) equation. Historically, the FRW method has not been applied to the solution of the NPB equation and other important nonlinear equations. This can be attributed to the absence of analytical expressions for volumetric Green's functions. Previous studies [1] using the FRW method have examined only the linearized Poisson-Boltzmann equation. Approximate volumetric Green's functions have been derived with the help of perturbation theory, and these expressions have been incorporated within the FRW framework. A unique advantage of this algorithm is that it requires no discretization of either the volume or the surface of the problem domains. Furthermore, each random walk is independent, so that the computational procedure is highly parallelizable. In our previous work [2, 3], we have presented preliminary results for our newly developed one- and two-dimensional FRW algorithm. We now present the results of the parallelization of the two-dimensional algorithm, with its finite-difference based validation. The solution of the NPB equation has many interesting applications, including the modeling of plasma discharges, semiconductor device modeling and the modeling of biomolecular structures and dynamics.

*Support for Dr. K. Chatterjee was provided under a National Research Council Summer Faculty Fellowship at the Air Force Research Laboratory, Wright-Patterson Air Force Base. Additional support was provided by the Air Force Office of Scientific Research, under grants monitored by Dr. J. Schmisser and Dr. F. Fahroo. We would like to acknowledge valuable discussions with Dr. M. D. White and Dr. D. V. Gaitonde.

REFERENCES

1. Co, H. and M. Mascagni, "Efficient modified 'walk on spheres' algorithm for the linearized poisson-boltzmann equation," *App. Phys. Lett.*, Vol. 78, No. 6, 787–789, 2001.
2. Chatterjee, K. and J. Poggie, "A meshless stochastic algorithm for the solution of the nonlinear Poisson-Boltzmann equation in the context of discharge modeling: 1D analytical benchmark," *AIAA Paper 2005-5339 in Proceedings of the 17th AIAA Computational Fluid Dynamics Conference*, Toronto, Ontario, Canada, 6–9, June, 2005.
3. Chatterjee, K. and J. Poggie, "A two-dimensional floating random walk algorithm for the numerical solution of the nonlinear Poisson-Boltzmann equation: Application to the modeling of plasma sheaths," *Proceedings of the 3rd MIT Conference on Computational Fluid and Solid Mechanics*, 1058–1061, Cambridge, MA, June 14–17, 2005. Elsevier: Oxford, UK, 2005.

Reduction of FDTD Simulation Time with Modal Methods

D. A. Gorodetsky and P. A. Wilsey
University of Cincinnati, USA

Abstract—In order to simulate electromagnetic phenomena at high frequencies, full wave solvers such as the FDTD method must be used. An alternative to the conventional FDTD method is to compute the zero state response with convolution. Convolution results in an increased computation time with every time step. By performing eigenmodal decomposition of the inputs, a constant time for the convolution can be achieved. We show how the solution can be constructed analytically in terms of the eigenvalues and the eigenvectors of the state transition matrix.

1. Introduction

FDTD is an evolutionary scheme that solves Maxwell's equations in the time domain [1, 2]. The evolution continues until steady state or stability in the output is achieved. Schemes of this type are often used when the analytical solution to an electromagnetic problem is prohibitive. Problems to be solved with FDTD are abundant in simulations of aircraft radar cross section at high frequency, microwave ICs, optical pulse propagation, antennas, bioelectromagnetic systems, bodies of revolution, etc. [1]. Situations where it is important to model on-chip interconnect include various microwave circuits such as amplifiers and optoelectronic circuits fabricated in CMOS technology. Reference [3] discusses the design of on-chip waveguides at optical frequencies and reference [4] discusses microwave frequencies. Such real-life problems often require grids with very large numbers of points, due to fine features of the simulated objects and high excitation frequencies. The end result of the fine grids is unreasonable simulation time. With the method proposed in this paper it may be possible to reduce this simulation time to a more acceptable level.

The starting point for the FDTD solution can be the initial conditions, such as an excitation signal. If the solution grid is partitioned into sub grids (i.e., for distributed computation) each containing N field variables, then the starting point is either the initial conditions or the inputs from the adjacent sub grids. We use the $N \times 1$ vector $\mathbf{Q}(n)$ to denote the state of every electric and magnetic field variable in the sub grid. The $N \times N$ state transition matrix $\mathbf{A}(n-i)$ is used to obtain the state at time n from the state at time i . We also define the $N \times 1$ input vector $\mathbf{X}(n)$, to represent the inputs to the sub grid at time n . The manipulation of these matrices in order to get the output of the sub grid, also called a module, was discussed in [5] and only the basic results are given here.

If the inputs are combined in $\mathbf{X}(n)$, an $I \times 1$ vector, then $\mathbf{Y}(n)$, the $O \times 1$ output vector of the module is given as:

$$\mathbf{Y}(n) = [\mathbf{CA}(n)\mathbf{B}] * \mathbf{X}(n) \quad (1)$$

where the $*$ symbol represents convolution, and the term in brackets is the impulse response $\mathbf{h}(n)$ of the FDTD module. From the results in [5] and from Equation (1) we can observe that the computing time grows with every time step, due to the properties of convolution. Therefore this method is useful only at early stages in the simulation when the number of inputs is small, and the convolution workload does not exceed the time to simulate the module with the standard FDTD.

A strategy to overcome this limitation for the TLM method was discussed in [6]. It involves writing each entry in the location (i, o) of the impulse response matrix as a sum of the eigenvalues of the state transition matrix as follows:

$$h(i, o, n) = \sum_{p=1}^P b_{iop} \lambda_p^n = \sum_{p=1}^P b_{iop} |\lambda_p|^n e^{j\omega_p n \Delta t} \quad (2)$$

This can be interpreted as the sum of P matrices, each modulated by a different eigenvalue λ_p . Instead of requiring the storage of the entire history of the inputs, this method requires storage of P matrices, where P is some fraction of N , as will be described later in this paper. This method takes a constant amount of time for every time step of the algorithm, with the number of multiplications given by IOP . In this paper we propose an alternative method that involves decomposing the input vector into a sum of eigenvectors. With the proposed method, the number of multiplications is reduced to OP .

2. Proposed Method

A technique to express the state $\mathbf{Q}(n)$ as a superposition of eigenvectors and to solve for the zero-input response was discussed in [7]. We propose the extension of that work to the zero-state response. In [7] the initial state is written as:

$$\mathbf{Q}(0) = a_0\mathbf{y}_0 + a_1\mathbf{y}_1 + \dots + a_N\mathbf{y}_N \quad (3)$$

where \mathbf{y}_k are the eigenvectors of the state transition matrix. Using Equation (3), the evolution in time can be expressed as:

$$\mathbf{Q}(n) = (\lambda_0)^n a_0\mathbf{y}_0 + (\lambda_1)^n a_1\mathbf{y}_1 + \dots + (\lambda_N)^n a_N\mathbf{y}_N \quad (4)$$

Our modification involves expressing the inputs as follows:

$$\begin{aligned} \mathbf{X}(0) &= a_{00}\mathbf{y}_0 + a_{01}\mathbf{y}_1 + \dots + a_{0N}\mathbf{y}_N \\ \mathbf{X}(1) &= a_{10}\mathbf{y}_0 + a_{11}\mathbf{y}_1 + \dots + a_{1N}\mathbf{y}_N \\ &\quad \dots \\ &\quad \dots \\ \mathbf{X}(T) &= a_{T0}\mathbf{y}_0 + a_{T1}\mathbf{y}_1 + \dots + a_{TN}\mathbf{y}_N \end{aligned} \quad (5)$$

With the inputs expressed as in Equation (5), the convolution will involve keeping only a sum for each column as shown below:

$$\begin{aligned} \mathbf{Y}(1) &= \mathbf{h}(1)\mathbf{X}(0) \\ &= \lambda_0 a_{00}\mathbf{y}_0 + \lambda_1 a_{01}\mathbf{y}_1 + \dots + \lambda_N a_{0N}\mathbf{y}_N \\ &= s_{10}\mathbf{y}_0 + s_{11}\mathbf{y}_1 + \dots + s_{1N}\mathbf{y}_N \end{aligned} \quad \begin{aligned} \mathbf{Y}(2) &= \mathbf{h}(2)\mathbf{X}(0) + \mathbf{h}(1)\mathbf{X}(1) \\ &= \lambda_0 s_{10}\mathbf{y}_0 + \lambda_1 s_{11}\mathbf{y}_1 + \dots + \lambda_N s_{1N}\mathbf{y}_N \\ &\quad + \lambda_0 a_{10}\mathbf{y}_0 + \lambda_1 a_{11}\mathbf{y}_1 + \dots + \lambda_N a_{1N}\mathbf{y}_N \\ &= s_{20}\mathbf{y}_0 + s_{21}\mathbf{y}_1 + \dots + s_{2N}\mathbf{y}_N \end{aligned} \quad (6)$$

From Equation (6) it is clear that a running sum of each column is kept and that convolution involves the multiplication of each column by its eigenvalue. In general the number of multiplications will depend on the number of entries in the \mathbf{y}_k vectors and N , the total number of points in the module. Assuming that P out of N eigenvectors are kept for the solution and the remaining ones are discarded, that the size of \mathbf{Y} is $O \times 1$, thus the number of multiplications per time step is reduced to OP .

The complex eigenvalues have a non-zero characteristic frequency obtained by finding the phase angle of the eigenvalue and indicated by $\Omega_i = 2\pi f_i$. The corresponding frequency domain frequency is given by $\omega_i = \Omega_i/\Delta t$ [7]. By properly selecting p , eigenmodes that satisfy the criteria $\Omega_i > 2\pi p$ can be eliminated since it is known that the discretization mechanism of the numerical simulation does not properly propagate these higher frequencies [9]. Adhering to the constraint that only wavelengths that are greater than 10 times the length of a side of a cell can be propagated allows p to be set at 1/10. After the elimination, P indicates the number of remaining eigenmodes.

Hence, the storage of the complex eigenvectors will take up the equivalent of $2OPk_1$ bytes, where k_1 is the number of bytes per double. As can be seen from Equation (6), during every time step two multiplications must be performed for every complex double that is stored. Also, the solution of Equation (5) requires $4OPk_1$ multiplications because the coefficients will in general be complex. Therefore, neglecting additions, every cycle will take roughly $8OPk_2$ milliseconds, where k_2 is the time per multiplication.

3. Results

A module with one interface was analyzed. The dimensions of this module were $1 \times 20 \times 2$ cells. Because the field was assumed zero on the boundary, the module contained only 175 points that participated in the calculation. This resulted in 175 eigenvalues, 116 of which consisted of 58 complex conjugate pairs while the remaining ones were either zero or unity and could be discarded. By setting $p = 0.1$, all but one of the complex conjugate pairs were discarded.

The module was attached to the terminating face a parallel plate waveguide structure that was simulated with the conventional FDTD and with the algorithm presented in this paper. At the excitation face a constant plane wave source of 10 GHz. was introduced. The dimensions of the waveguide without the module were $58 \times 20 \times 2$ cells, which translates to the dimensions of $2 \times 0.0229 \times 0.002$ wavelengths at 10 GHz. The electric field at various points along the length of the waveguide was obtained for the first 10,000 iterations. The results were always virtually identical between the conventional FDTD and our methods. In Figure 1 the electric field

variation with time in cell (29, 10, 1) is shown. Figure 2 demonstrates that the simulation results match the predictions from electromagnetic theory.

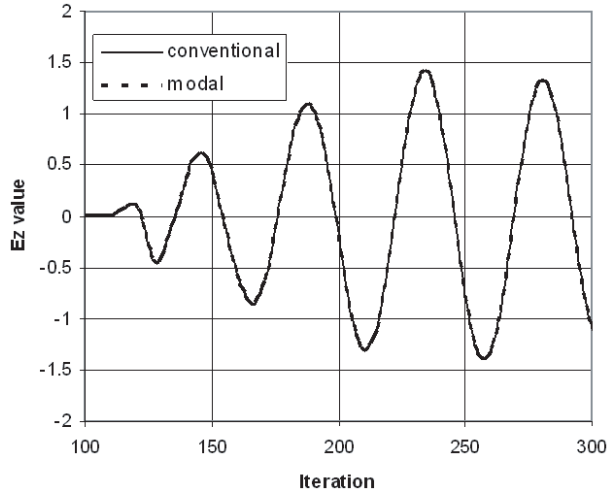


Figure 1: Comparison of results of conventional and proposed methods. The point is located in the middle of the waveguide.

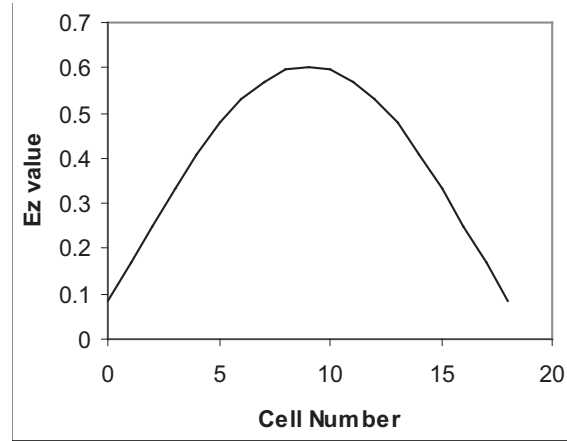


Figure 2: The electric field in the transverse direction. The results correctly indicate the presence of the TM_0 mode.

In order to demonstrate the case when the results were not identical, a module with dimensions of $3 \times 20 \times 2$ cells was utilized. This translated to 525 points. In order to get accurate results from the larger module, p had to be increased to 0.14 in this case. This caused the final system to end up with 16 complex conjugate pairs. The electric field variation in the cell adjacent to the excitation face of the waveguide is displayed in Figure 3. The comparison with the situation where the module produces zero output proves the functionality of the module. Figure 4 shows the small difference between the output of the module at its interface and the electric field produced by the conventional FDTD method at the same point. This difference is barely noticeable in the beginning of the simulation and increases as the simulation progresses in time.

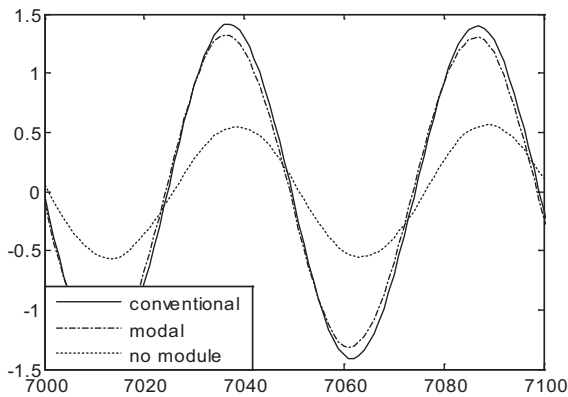


Figure 3: The electric field (E_z) near the waveguide entrance. The overall effect of the module on the simulation can be observed.

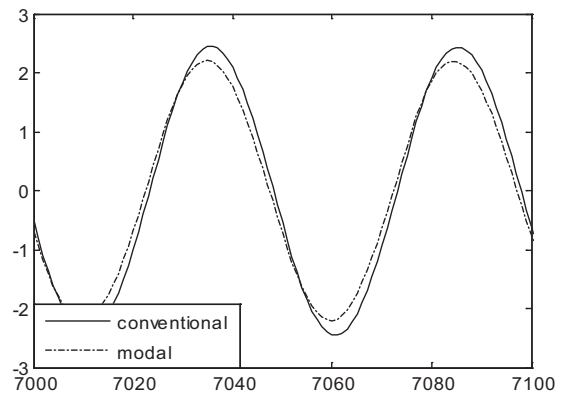


Figure 4: The electric field at the module interface.

4. Conclusion

In this paper we discussed the full-wave simulation of interconnect that is found on high frequency integrated circuits. To speed up the simulation, we developed a recursive algorithm for convolution. This recursive algorithm is based on the modal decomposition approach to the impulse response of the finite-difference time-

domain numerical simulation. Its advantages over an earlier approach [5] is that the storage of the history of the impulse responses (IOT) is no longer required. The only storage required is that of the eigenvectors ($2OP$), eigenvalues ($2P$), and coefficients ($2P$). Another improvement over [5] is that the storage of the inputs (IT) is replaced by the much smaller storage of the coefficients. In regards to the approach published in [6], the storage requirement is improved from $\sim (IOP)$ to $\sim (OP)$ and the number of multiplications per time step is improved in the same manner.

The methods discussed in this paper for interconnect can be extended to a majority of other electromagnetic simulation scenarios such as antennas and radar cross section simulation. An important application is the use of the FDTD method to simulate the propagation of electromagnetic waves in semiconductor devices. This is done by coupling the electron transport equations with Maxwell's equations [10].

Future work will involve the investigation into the techniques, such as change of basis, with which multiple modules can be combined together to reduce the overall simulation time. As was seen in the results, the relationship between the N and P varies with the size of the module as well as the choice of p . More insight into this relationship will be required in order to be able to optimize the module for speed or accuracy requirements.

REFERENCES

1. Taflove, A. and S. C. Hagness, *Computational Electrodynamics: The Finite-Difference Time-Domain Method, Second Edition*, Artech House, Boston, 2000.
2. De Moura, C. A., "Non-sequential numerical algorithms for time marching models," *RT06/99, IC-UFF*, July 1999.
3. Fullin, E., G. Voirin, M. Chevroulet, A. Lagos, and J. M. Moret, "CMOS-based technology for integrated optoelectronics: a modular approach," *IEEE International Electron Devices Meeting*, 527–530, 1994.
4. Kim, B.-K., B.-K. Ko, K. Lee, J.-W. Jeong, K.-S. Lee, and S.-C. Kim, "Monolithic planar RF inductor and waveguide structures on silicon with performance comparable to those in GaAs MMIC," *IEEE International Electron Devices Meeting*, 717–720, 1995.
5. Gorodetsky, D. A. and P. A. Wilsey, "A signal processing approach to finite-difference time-domain computations," *IEEE International Midwest Symposium on Circuits and Systems*, 2005.
6. Chen, Z., "Analytic Johnson's matrix and its application in TLM diakoptics," *IEEE MTT-S Digest*, Vol. 2, 777–780, 1995.
7. Chen, Z. and P. P. Silvester, "Analytic solutions for the finite-difference time-domain and transmission-line-matrix methods," *Microwave and Optical Technology Letters*, Vol. 7, No. 1, 5–8, 1994.
8. Grossman, S. I., *Elementary Linear Algebra*, Saunders College Publishing, Fort Worth, 1994.
9. Kunz, K. S. and R. J. Luebbers, *The Finite Difference Time Domain Method for Electromagnetics*, CRC Press, Boca Raton, 1993.
10. El-Ghazaly, S. M. and T. Itoh, "Electromagnetic interfacing of semiconductor devices and circuits," *IEEE MTT-S International Microwave Symposium Digest*, Vol. 1, 151–154, 1997.

Approximate Decomposition for the Solution of Boundary Value Problems for Elliptic Systems Arising in Mathematical Models of Layered Structures

Y. Shestopalov and N. Kotik
Karlstad University, Sweden

Abstract—We present an alternative approach to the solution of boundary value problems (BVPs) for elliptic systems arising in mathematical models of layered structures. The main idea of the method is to consider auxiliary problems for differential operators separated componentwise and to reduce them to a sequence of iterative problems such that each can be solved (explicitly) by the Fourier method. The solution sequence is then constructed with the help of a contracting transfer operator evaluated explicitly. This method facilitates both analytic and numerical solutions and can be generalized to more complicated mixed BVPs for semilinear partial differential operators.

1. Introduction

The processes which take place in layered structures may be described in terms of boundary value problems (BVPs) for elliptic systems [1, 2], among them are the Laplace, Helmholtz, and Lamè equations, equipped with appropriate boundary conditions of mixed type, including boundary–value contact problems (BVCPs) formulated and investigated in [3].

The simplest examples of BVPs with boundary conditions of mixed type in electromagnetics and acoustics [1, 2] arise when the Dirichlet (or Neumann) conditions are stated on one part of the boundary and the Neumann (Dirichlet) condition on its complement. Such problem are formulated, e. g., in mathematical models of the wave propagation in transmission lines [1]. A decomposition for the solution to the BVPs for the equation systems can be applied when the differential operator can be separated while the boundary value (trace) operators are mixed componentwise on the boundary. In Section 3 we present an example of such a separation (decomposition).

In this work we present an approach for analytical and numerical solution of BVPs in thin layers based on approximate decomposition. The main idea of this method is to simplify the general BVP and to reduce it to a chain of auxiliary problems and then to a sequence of iterative problems such that each of them can be solved (explicitly) by the Fourier method.

2. Formulation

We present the method for the case of a BVCP [3] for the system of Lamè equations in a thin layer (band) equipped with mixed boundary conditions. To this end, consider an elastic band $S = \{-\infty < x_1 < +\infty, 0 < x_2 < h\}$ with Poisson's ratio ν situated on the stiff base $x_2 \equiv 0$. The boundary lines $x_2 = h$ and $x_2 \equiv 0$ are denoted, respectively, by \mathcal{K}_1 and \mathcal{K}_2 (Fig. 1); $\omega = \bigcup_{m=1}^N \omega_m$, where $\omega_m = [a_m, b_m]$, is a set of disjoint segments; and $\omega^* = \mathcal{K}_1 \setminus \omega$. Distribution of shearing strains on line \mathcal{K}_1 , displacements on ω , and elongations on ω^* are given. We denote by u_j and \mathcal{F}_j , ($j = 1, 2$) the displacements and respectively projections of the body forces in directions x_j . The determination of u_j reduces to a mixed BVP [3] for the Lamè equations in S

$$\Delta u_j + k_0 \frac{\partial}{\partial x_j} \left(\frac{\partial u_1}{\partial x_1} + \frac{\partial u_2}{\partial x_2} \right) = \mathcal{F}_j, \quad k_0 = \frac{1}{1 - 2\nu}, \quad j = 1, 2 \quad (1)$$

with the boundary conditions

$$\begin{aligned} u_2 = 0, \quad \frac{\partial u_1}{\partial x_2} + \frac{\partial u_2}{\partial x_1} = 0 & \quad \text{on } \mathcal{K}_2, \\ \frac{\partial u_2}{\partial x_1} + \frac{\partial u_1}{\partial x_2} = f_1(x_1) & \quad \text{on } \mathcal{K}_1, \\ u_2 = f_2(x_1) & \quad \text{on } \omega, \\ (k_0 - 1) \frac{\partial u_1}{\partial x_1} + (k_0 + 1) \frac{\partial u_2}{\partial x_2} = f_3(x_1) & \quad \text{on } \omega^* \end{aligned} \quad (2)$$

and the conditions at infinity

$$\begin{aligned} \Phi_s(u_1, u_2) &= \int_S \Pi_S ds < \infty, \\ \Pi_s &= (k_0 - 1) \left(\sum_{j=1}^2 \frac{\partial u_j}{\partial x_j} \right)^2 + 2 \sum_{j=1}^2 \left(\frac{\partial u_j}{\partial x_j} \right)^2 + \left(\frac{\partial u_1}{\partial x_2} + \frac{\partial u_2}{\partial x_1} \right)^2, \end{aligned} \tag{3}$$

BVP (1)–(3) has the unique classical solution if the boundary functions are sufficiently smooth. Namely, the following statement is valid (see [3]):

If the functions $\mathcal{F}_1 \in L_p(S)$, $\mathcal{F}_2 \in L_p(S)$, $f_1 \in L_p(\mathcal{K}_1)$, $f_3 \in L_p(\omega^*)$, $p > 1$ ($f \in L_p(\Omega)$ if $|f|^p$ is integrable over Ω) and function $f_2 \in C^q(\mathcal{K}_1)$, $q \geq 3$, is a smooth (q -times continuously differentiable) compactly-supported function with $supp f_2 \in \omega$ then problem (1)–(3) is uniquely solvable if and only if

$$\int_{\mathcal{K}_1} f_1 dx_1 + \int_S \mathcal{F}_1 dS = 0$$

and the solutions $u_j \in C^2(\Pi_{ah}) \cap C(\bar{\Pi}_{ah})$ in every rectangle $\Pi = \Pi_{ah} = \{(x_1, x_2) : 0 < x_1 < a, 0 < x_2 < h\}$.

3. Approximate Decomposition

Consider a simplified version of the problem (1)–(3) which will be called *problem A*: body forces $\mathcal{F}_1, \mathcal{F}_2 \equiv 0$; shearing stresses $f_1 \equiv 0$ on \mathcal{K}_2 ; and normal stresses $f_3 \equiv 0$ on ω^* . Consider this problem in a long rectangle Π_{ah} bounded by the curve $\Gamma = \hat{\mathcal{K}}_1 \cup \hat{\mathcal{K}}_2 \cup \mathcal{H}_1 \cup \mathcal{H}_2$, where $\hat{\mathcal{K}}_i = \mathcal{K}_i \cap \{0 < x_1 < a\}$, ($i = 1, 2$); $\hat{\omega}^* = \omega^* \cap \{0 < x_1 < a\}$; $\mathcal{H}_1 = \{\mathbf{x} = (x_1, x_2) : x_1 = 0, 0 < x_2 < h\}$, $\mathcal{H}_2 = \{\mathbf{x} = (x_1, x_2) : x_1 = a, 0 < x_2 < h\}$; and $\mathbf{u} = (u_1, u_2)$ denotes the vector of displacements. Introduce the trace operators $L^{(1)}$ and $L^{(2)}$ specifying the boundary conditions on $\hat{\omega}$, $\hat{\omega}^*$ and Γ :

$$\begin{aligned} L^{(1)}\mathbf{u} &= \begin{pmatrix} l_{11}^{(1)} & 0 \\ 0 & l_{22}^{(1)} \end{pmatrix} \mathbf{u}, \\ l_{11}^{(1)}u_1 &= \frac{\partial u_1}{\partial \nu} (\mathbf{x} \in \Gamma), \quad l_{22}^{(1)}u_2 = u_2 \quad (\mathbf{x} \in \omega \cup \hat{\mathcal{K}}_2 \cup \mathcal{H}_1 \cup \mathcal{H}_2) \end{aligned} \tag{4}$$

is the operator of the Neumann–Dirichlet boundary conditions, and

$$\begin{aligned} L^{(2)}\mathbf{u} &= \begin{pmatrix} l_{11}^{(2)} & l_{12}^{(2)} \\ l_{21}^{(2)} & l_{22}^{(2)} \end{pmatrix} \mathbf{u}, \\ l_{11}^{(2)}u_1 &= 0, \quad l_{12}^{(2)}u_2 = \frac{\partial u_2}{\partial \tau} \quad (\mathbf{x} \in \Gamma), \\ l_{21}^{(2)}u_1 &= \alpha u_{1,1} \quad l_{22}^{(2)}u_2 = u_{2,2} \quad (\mathbf{x} \in \hat{\omega}^*), \end{aligned} \tag{5}$$

where

$$\frac{\partial}{\partial \tau} = \begin{cases} \frac{\partial}{\partial x_1}, & \mathbf{x} \in \mathcal{K}_1 \cup \mathcal{K}_2 \\ \frac{\partial}{\partial x_2}, & \mathbf{x} \in \mathcal{H}_1 \cup \mathcal{H}_2 \end{cases}, \quad \frac{\partial}{\partial \nu} = \begin{cases} (-1)^i \frac{\partial}{\partial x_2}, & \mathbf{x} \in \mathcal{K}_i \\ (-1)^i \frac{\partial}{\partial x_1}, & \mathbf{x} \in \mathcal{H}_i \end{cases}, \quad \alpha = \frac{k_0 + 1}{k_0 - 1}. \tag{6}$$

The operator $L\mathbf{u} = L^{(1)}\mathbf{u} + L^{(2)}\mathbf{u}$ specifies the boundary conditions of problem A in the form $L\mathbf{u} = \mathbf{f}$, with $\mathbf{f} = (0, f_2(\mathbf{x}))$ and

$$\hat{f}_2(\mathbf{x}) = \begin{cases} f_2(x_1), & \mathbf{x} = (h, x_1) \in \omega, \\ 0, & \mathbf{x} \in \Gamma \setminus \omega, \end{cases} \tag{7}$$

being a differentiable function on Γ with a compact support $supp f_2 \subseteq \omega$. Introduce matrix differential operators of the system in problem (1)–(3) and problem A and rewrite the latter as

$$\mathcal{D}\mathbf{u} = 0, \quad L\mathbf{u} = \mathbf{f}, \tag{8}$$

where

$$\begin{aligned} \mathcal{D} &= \Delta + k_0 A, & \Delta &= \begin{pmatrix} \Delta_1 & 0 \\ 0 & \Delta_2 \end{pmatrix}, \\ \Delta_1 u_1 &= (k_0 + 1) \frac{\partial^2 u_1}{\partial x_1^2} + \frac{\partial^2 u_1}{\partial x_2^2}, & \Delta_2 u_2 &= \frac{\partial^2 u_2}{\partial x_1^2} + (k_0 + 1) \frac{\partial^2 u_2}{\partial x_2^2}, \\ A &= \begin{pmatrix} 0 & 1 \\ 1 & 0 \end{pmatrix} \frac{\partial^2}{\partial x_1 \partial x_2}, & \mathbf{f} &= (0, \widehat{f}_2(\mathbf{x})). \end{aligned} \quad (9)$$

Assuming that displacements u_2 are absent on ω^* write problem A in the form

$$\mathcal{D}\mathbf{u} = 0, \quad \widehat{L}\mathbf{u} = \mathbf{f}, \quad \widehat{L} = \widehat{L}^{(1)} + \widehat{L}^{(2)}, \quad (10)$$

where $\widehat{L}^{(1)} = \|\widehat{l}_{ii}^{(1)}\|_{i=1,2}$ is defined as in (4) with the only difference that $\widehat{l}_{22}^{(1)} u_2 = \frac{1}{2} u_2$, $\mathbf{x} \in \Gamma$, and $\widehat{L}^{(2)}$ has two nontrivial components: $\widehat{l}_{21}^{(2)}$ defined in (5) and $\widehat{l}_{22}^{(2)} u_2 = \frac{1}{2} u_2$, $\mathbf{x} \in \Gamma$.

Define the sequence $\{\mathbf{u}_n\}$ of vector-functions according to

$$\begin{aligned} \Delta \mathbf{u}_0 &= 0, & \widehat{L}^{(1)} \mathbf{u}_0 &= \mathbf{f}_0 = \left(-\frac{\partial \widehat{f}_2}{\partial x_1}, \widehat{f}_2(x_1) \right), & x_1 \in \omega, \\ \Delta \mathbf{u}_{n+1} &= -k_0 A \mathbf{u}_n, & \widehat{L}^{(1)} \mathbf{u}_{n+1} &= -\widehat{L}^{(2)} \mathbf{u}_n, & n = 0, 1, 2, \dots \end{aligned} \quad (11)$$

The limiting function (if exists) $\mathbf{u} = \lim_{n \rightarrow \infty} \mathbf{u}_n$ (where the limit is determined with respect to an appropriate norm) satisfies (8). In order to prove the existence consider BVP (11) for $\mathbf{u}_{n+1} = (u_1^{(n+1)}, u_2^{(n+1)})$. Componentwise, (11) consists of two inhomogeneous BVPs for Poisson equation in the rectangle. The solution to each problem can therefore be obtained as a sum of the corresponding volume and surface (line) potentials. In the vector-operator form the relationship between two intermediate problems (11) can be represented as

$$\mathbf{u}_{n+1} = \mathbf{K} \mathbf{u}_n, \quad (12)$$

where \mathbf{K} is a volume-surface integral operator defined in term of the potentials.

Applying the Schauder *a priori* estimates of the solution to BVPs for elliptic PDEs [4, 5], using the explicit form of \mathbf{u}_{n+1} and properties of logarithmic and Green's potentials [6, 7], one can show that

$$\|\mathbf{u}_{n+1}\|_{C^2(\Pi)} \leq M_n (\|\mathbf{u}_n\|_{C^2(\Pi)} + \|f_2\|_{C^2(\omega)}), \quad n = 1, 2, \dots, \quad (13)$$

where constant M_n depends on the diameter of Π_{ah} and $M_n \rightarrow 0$ if $\text{diam } \Pi_{ah} \rightarrow 0$. Thus, operator \mathbf{K} (12) is a contraction in the space $C^2(\Pi) \cap C(\bar{\Pi})$ of two-component vector-functions if the diameter of set ω , parameter h , and the norm of boundary function f_2 are sufficiently small. This implies the existence of the unique solution $\mathbf{u} \in C^2(\Pi) \cap C(\bar{\Pi})$ to problem A.

This approximate decomposition can be applied to the solution of BVPs of the type (1), (2) for semilinear systems with the differential operators $\mathcal{D}\mathbf{u} = \Delta \mathbf{u} + \mathcal{F}(\mathbf{u}, \mathbf{u}_{x_1}, \mathbf{u}_{x_2}, \mathbf{u}_{x_1 x_2})$, where \mathcal{F} is nonlinear with respect to \mathbf{u} and \mathbf{u}_{x_i} . Constructing the iterations similar to (11) or (12) and showing or assuming that the corresponding transfer operator \mathbf{K} is contraction, we obtain a recursive procedure (12) to determine displacements \mathbf{u} .

4. Solution by the Fourier Method

One can obtain explicit solution to every intermediate BVP (11) in the form of Fourier series

$$\begin{aligned} u_2^{(n+1)} &= \sum_{m=1}^{\infty} \sin \frac{\pi m}{a} x_1 \left(d_m \sinh \frac{\pi m \sqrt{k_0 + 1}}{a} x_2 + e_m \sinh \frac{\pi m}{a \sqrt{k_0 + 1}} x_2 \right), \\ u_1^{(n+1)} &= \sum_{m=1}^{\infty} \cos \frac{\pi m}{a} x_1 \left(g_m \cosh \frac{\pi m}{a \sqrt{k_0 + 1}} x_2 + q_m \cosh \frac{\pi m \sqrt{k_0 + 1}}{a} x_2 \right), \end{aligned} \quad (14)$$

where

$$a_m = -\frac{\sinh \frac{\pi m h}{a \sqrt{k_0 + 1}}}{\sinh \frac{\pi m h \sqrt{k_0 + 1}}{a}} b_m, \quad b_m = \frac{f_m}{\sinh \frac{\pi m h}{a \sqrt{k_0 + 1}}}, \quad (15)$$

$f_m = \frac{2}{a} \int_0^a f_2(x_1) \sin \frac{\pi m}{a} dx_1$ are Fourier coefficients for the function f_2 from boundary condition (2) and

$$\begin{aligned} d_m &= \frac{\sqrt{k_0 + 1}}{k_0 + 2} b_m, & e_m &= \left(1 + \frac{\sqrt{k_0 + 1}}{k_0 + 2}\right) b_m, \\ g_m &= \frac{\sqrt{k_0 + 1}}{k_0 + 2} b_m, & q_m &= \frac{k_0 + 3}{(k_0 + 2)\sqrt{k_0 + 1}} a_m b_m \end{aligned} \tag{16}$$

are the Fourier coefficients obtained for (11) on the previous stage n .

Series (14) converge absolutely and uniformly in every rectangle $\Pi_{ah}^\delta = \{0 \leq x_1 \leq a, \delta \leq x_2 \leq h\}$ with $0 < \delta < h$ and admit term-wise differentiation arbitrary number of times. The rate of convergence is exponential.

In view of the explicit solution (14) it is reasonable to specify a boundary function $f_2(x_1)$ in problem A and (7) as a smooth compactly-supported function $f_2 \in C^p(R)$, $p \geq 3$, with $supp f_2 \in \omega$. One can consider, for example, the case when $f_2(x_1)$ is the so-called hat function of order p (a product of a polynomial in even powers of argument that vanishes at the endpoints of ω and a Gaussian exponent) for which the Fourier coefficients can be calculated explicitly. Such hat functions possess the properties of B-splines; therefore, one can approximate or interpolate a smooth function on the line R with a finite support ω by a finite linear combination of hat functions and apply the approximate decomposition with rapidly converging series solutions to BVPs with virtually arbitrary boundary functions.

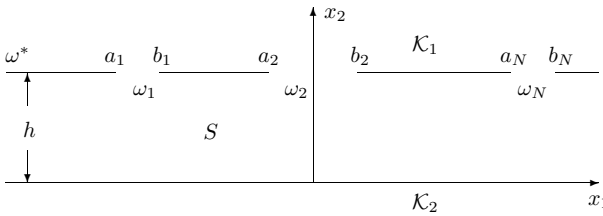


Figure 1: Statement of the problem.

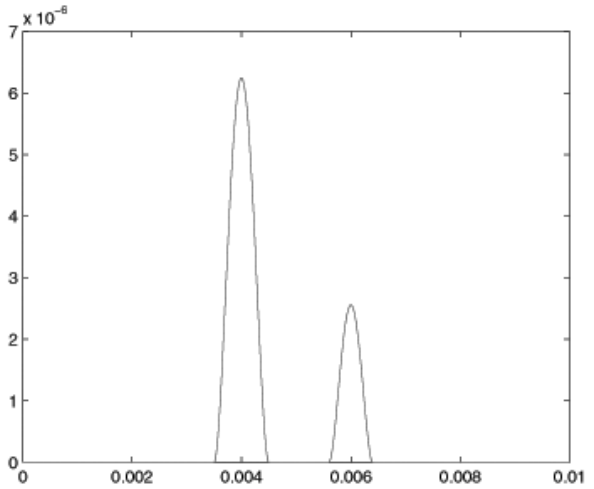


Figure 2: The function f_2 .

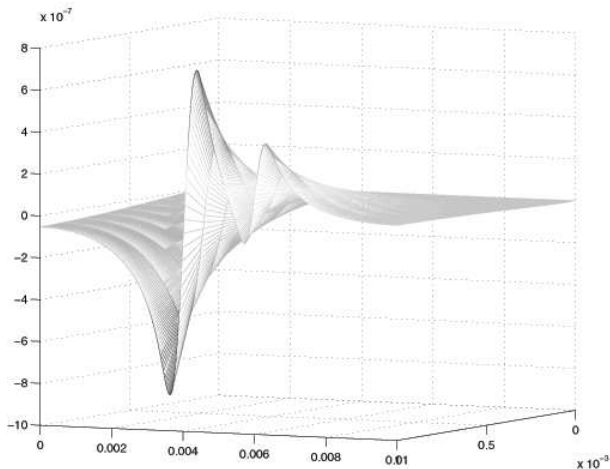


Figure 3: The displacement u_1 .

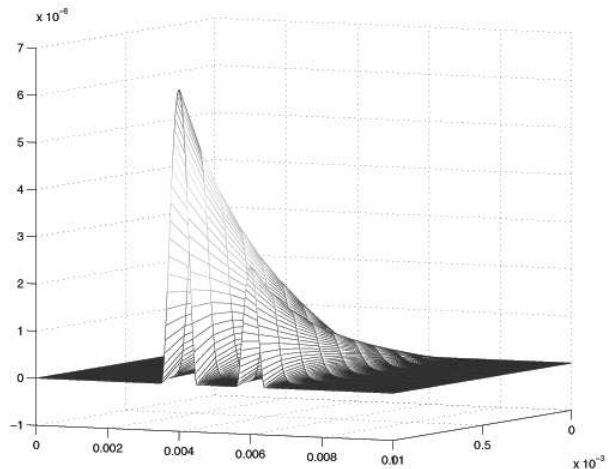


Figure 4: The displacement u_2 .

5. Numerical

Let us present some qualitative results of numerical–analytical solution to problem A (a simplified version of (1)–(3) considered in a long rectangle) obtained using approximate decomposition (first iteration); the profiles of boundary displacements are taken as hat functions presented in Fig. 2. Figs 3 and 4 show u_1 and u_2 calculated in the case of $a/h = 10$ and two disjoint segments $\omega = \cup_{i=1}^2 [x_{S_i} - p_i, x_{S_i} + p_i]$.

Values of displacement u_1 in Fig. 3 are zero at $x_{S_{1,2}}$ because these points shift only in x_2 -direction; values in the support intervals $(x_{S_1} - p_1, x_{S_1})$ and $(x_{S_2} - p_2, x_{S_2})$ are negative because these points shift in the opposite direction; values in the intervals $(x_{S_1}, x_{S_1} + p_1)$ and $(x_{S_2}, x_{S_2} + p_2)$ are positive because these points also shift in the x_2 -direction and take maximum and minimum at the respective points. Function u_2 in Fig. 4 takes only positive values in the intervals $(x_{S_1} - p_1, x_{S_1} + p_1)$ and $(x_{S_2} - p_2, x_{S_2} + p_2)$, maximum and minimum are at the points x_{S_1} and x_{S_2} respectively.

6. Conclusion

We have developed a method of approximate analytical–numerical solution to BVPs for elliptic system in parallel-plane layers based on decomposition of boundary value conditions. An advantage of the method is the possibility of explicit determination and fast computation and visualization of all components at every point of the layer. The method can be extended to wide families of BVPs using spline-type approximations based on hat functions.

Acknowledgment

The work is supported by the TryckTeknisk Forskning (T2F) program. We would like to thank Dr Magnus Lestelius and Dr Peter Rättö from the Department for Chemistry of the Karlstad University (Sweden) for valuable discussions.

REFERENCES

1. Shestopalov, Y., E. Chernokozhin, and Y. Smirnov, *Logarithmic Integral Equations in Electromagnetics*, VSP Int. Science Publishers, Utrecht, Boston, Köln, Tokyo, 2000.
2. Smirnov, Y., H. W. Schürmann, and Y. Shestopalov, “Propagation of TE-waves in cylindrical nonlinear dielectric waveguides,” *Physical Review E*, Vol. 71, 0166141–10, 2005.
3. Vorovich, I. I., V. M. Alexandrov, and V. A. Babeshko, *Non-classical Problems in Elasticity Theory*, Nauka Moscow, 1974.
4. Schauder, J., “Über Lineare elliptische differentialgleichungen zweiter ordnung,” *Math. Z.*, Vol. 38, 257–282, 1934.
5. Bers, L., F. John, and M. Schechter, *Partial Differential Equations*, New York, 1964.
6. Tikhonov, A. N. and A. A. Samarskii, *Equations of Mathematical Physics*, Moscow, Nauka, 1972.
7. Shestopalov, Y., “Application of the method of generalized potentials in some problems of wave propagation and diffraction,” *Zh. Vych. Mat. Mat. Fiz.*, Vol. 30, 1081–1092, 1990.

Generation of Diverse Time-series Data though Monitoring a Death-multiple Immigration Population Model

J. O. Matthews, K. I. Hopcraft, and E. Jakeman
University of Nottingham, UK

Discrete population models have been employed in combination with random walk techniques to model successfully non-Gaussian clutter occurring in coherent imaging systems [e.g., 1, 2]. The method models the coherent returns from an ensemble of scatterers as a random walk comprising a fluctuating number of steps. Non-Gaussian limiting distributions obtain when the stochastic process describing the discrete distribution is subject to clustering. In particular, a simple mathematical paradigm for turbulence is the birth-death-immigration process, where turbulent eddies nucleate (immigration), are shed (birth) and dissipate (death). The equilibrium distribution is then of the negative binomial class, this being the discrete analogue of continuous gamma-distributed fluctuations, and the clutter is then K -distributed [2]. Here we discuss the properties of a death-multiple immigration model [3], which allows for pairs, triplets, \dots n -tuplets to enter the population, and which has the useful property of enabling a very wide class of equilibrium distributions to be constructed, including the negative-binomial class and distributions with scale free-characteristics. Allowing “individuals” to leave the population creates a series of events in time [4], whose characteristics can be tailored to exhibit a wide range of behaviours, together with correlation properties including non-Poissonian processes and fractals. The utility to model non-Gaussian fractal processes using the technique will be discussed [5], together with the wider implications for the generation of time series.

REFERENCES

1. Jakeman, E. and P. N. Pusey, “A model for non-rayleigh sea echo,” *IEEE Trans. Antennas and Propagation*, Vol. 24, 807–814, 1976.
2. Jakeman, E., “On the statistics of K -distributed noise,” *J. Phys. A: Math. Gen*, Vol. 13, 31–38, 1980.
3. Matthews, J. O., K. I. Hopcraft, and E. Jakeman, “Generation and monitoring of discrete stable random processes using multiple immigration population models,” *J. Phys. A: Math. Gen*, Vol. 36, 11585–11603, 2003.
4. Jakeman, E., K. I. Hopcraft, and J. O. Matthews, “Distinguishing population processes by external monitoring,” *Proc. Roy. Soc. Lond. A*, Vol. 459, 623–639, 2003.
5. Jakeman, E., K. I. Hopcraft, and J. O. Matthews, “Fluctuations in a coupled population model,” *J. Phys. A: Math. Gen*, Vol. 38, 6447–6461, 2005.

Implementation of the PML in the CIP Method

Y. Ando and M. Hayakawa

The University of Electro-communications, Japan

The constrained interpolation profile (CIP) method, a numerical solver for multiphase problems, can be applied to electromagnetic problems. The method is based on the upwind scheme for the finite difference method, but the variables to be calculated are not only the values of the electromagnetic fields, but also the spatial derivatives. Those variables are used to interpolate the profiles between the grids by means of cubic polynomials, and to calculate them at the next time step with good precision.

Invoking the directional splitting in the Maxwells equations allows us to treat electromagnetic fields as two one-way waves in each direction, and to reduce them into advection equations. For example, in $\pm x$ -direction of a 2-dimensional problem with $\frac{\partial}{\partial z} = 0$, the equations in free-space are given by

$$\frac{\partial f^{\pm}(r, t)}{\partial t} \pm c \frac{\partial f^{\pm}(r, t)}{\partial x} = 0, \quad \frac{\partial g^{\pm}(r, t)}{\partial t} \pm c \frac{\partial g^{\pm}(r, t)}{\partial x} = 0, \quad (1)$$

where $f^{\pm}(r, t) = \sqrt{\epsilon} E_z \mp \sqrt{\mu} H_y$, $g^{\pm} = \frac{\partial f^{\pm}}{\partial x}$, and c is the velocity. The reduced equations can be solved by using CIP method.

The CIP method has an absorbing boundary condition (ABC) as good as the 1st Mur's ABC in its nature. But, it is necessary to develop the ABC with better performance if required. In this study, we examine the perfect matched layer (PML) in the CIP scheme.

The application is straightforward, but some considerations are necessary in the computation because the implementation yields non-advection terms:

$$\frac{\partial f^{\pm}(r, t)}{\partial t} \pm c \frac{\partial f^{\pm}(r, t)}{\partial x} = -s(x)f^{\pm}(r, t), \quad \frac{\partial g^{\pm}(r, t)}{\partial t} \pm c \frac{\partial g^{\pm}(r, t)}{\partial x} = -\frac{\partial\{s(x)f^{\pm}(r, t)\}}{\partial x}, \quad (2)$$

where $s(x)$ is the normalized conductivity of the PML. One of the solution is obtained by dividing the equations into advection phase:

$$\frac{\partial f^{\pm}(r, t)}{\partial t} \pm c \frac{\partial f^{\pm}(r, t)}{\partial x} = 0, \quad \frac{\partial g^{\pm}(r, t)}{\partial t} \pm c \frac{\partial g^{\pm}(r, t)}{\partial x} = 0, \quad (3)$$

and then, non-advection phase

$$\frac{\partial f^{\pm}(r, t)}{\partial t} = -s(x)f^{\pm}(r, t), \quad \frac{\partial g^{\pm}(r, t)}{\partial t} = -\frac{\partial\{s(x)f^{\pm}(r, t)\}}{\partial x} = -\frac{ds(x)}{dx}f^{\pm}(r, t) - s(x)g^{\pm}(r, t). \quad (4)$$

Let $f^{\pm,*}$ denote the results of advection phase. The first equation can be evaluated analytically:

$$f^{\pm, n+1} = f^{\pm,*} \cdot e^{-s(x)\Delta t}, \quad (5)$$

where $f^{\pm, n+1}$ stands for the value at the next times step. The evaluation of the second equation in Eq. (4) can be performed numerically:

$$g^{\pm, n+1} = g^{\pm,*} - \Delta t \left\{ -\frac{ds(x)}{dx} f^{\pm,*} - s(x)g^{\pm,*} \right\}. \quad (6)$$

The successful formulation of the PML in the CIP method enables us to absorb the outgoing waves as much as required by increasing the layers. The numerical experiments show the good performance of the present formulation.

Some Elliptic Traveling Wave Solutions to the Novikov-Veselov Equation

J. Nickel¹, V. S. Serov², and H. W. Schürmann¹

¹University of Osnabrück, Germany

²University of Oulu, Finland

Abstract—An approach is proposed to obtain some exact explicit solutions in terms of elliptic functions to the Novikov-Veselov equation (NVE[$V(x, y, t) = 0$]). An expansion ansatz $V \rightarrow \psi = \sum_{j=0}^2 a_j f^j$ is used to reduce the NVE to the ordinary differential equation $(f')^2 = R(f)$, where $R(f)$ is a fourth degree polynomial in f . The well-known solutions of $(f')^2 = R(f)$ lead to periodic and solitary wave like solutions V . Subject to certain conditions containing the parameters of the NVE and of the ansatz $V \rightarrow \psi$ the periodic solutions V can be used as start solutions to apply the (linear) superposition principle proposed by Khare and Sukhatme.

1. Introduction

The Novikov-Veselov (NV) equation [1] as a “natural” two-dimensional generalization of the celebrated Korteweg-de Vries (KV) equation [2] has relevance in nonlinear physics (in particular in inverse scattering theory) [3, 4] and mathematics (cf. e. g., [5, 6]).

As regards to physics, Tagami [3] derived solitary solutions of the NV equation by means of the Hirota method. Cheng [4] investigated the NV equation associated with the spectral problem $(\partial_x \partial_y + u)\psi = 0$ in the plane and presented solutions by applying the inverse scattering transform. With regards to mathematics, Taimanov [5] investigated applications of the (modified) NV equation to differential geometry of surfaces. Ferapontov [6] used the (stationary) NV equation to describe a certain class of surfaces in projective differential geometry (the so-called isothermally asymptotic surfaces).—Apart from these applications solutions of the NV equation are interesting in and of themselves.

In the following we derive some solutions of the NV equation by combining a symmetry reduction method [7, 8] and the Khare-Sukhatme superposition principle [9–12].

2. Elliptic Solutions

2.1. General Considerations

Following Novikov and Veselov [1] we consider the system

$$V_t = \partial^3 V + \bar{\partial}^3 V + 3\partial(uV) + 3\bar{\partial}(\bar{u}V), \quad (1)$$

$$\bar{\partial}u = \partial V, \quad (2)$$

where $\partial = \frac{1}{2}(\partial_x - i\partial_y)$, $\bar{\partial} = \frac{1}{2}(\partial_x + i\partial_y)$ are the Cauchy-Riemann operators in \mathbb{R}^2 . System (1), (2) is equivalent to

$$V_t = \frac{1}{4}(V_{xxx} - 3V_{xyy}) + 3V(u_{1x} + u_{2y}) + 3(u_1 V_x + u_2 V_y), \quad (3)$$

$$V_x = u_{1x} - u_{2y}, \quad -V_y = u_{1y} + u_{2x} \quad (4)$$

with $u(x, y, t) = u_1(x, y, t) + iu_2(x, y, t)$, where u is defined up to an arbitrary holomorphic function $\varphi = \varphi_1 + i\varphi_2$ so that $\varphi_{1x} = \varphi_{2y}$, $\varphi_{1y} = -\varphi_{2x}$. (4) imply

$$u_1 = -2\partial_x^{-1}\partial_y\tilde{D}V + V + \varphi_1, \quad u_2 = -2\tilde{D}V + \varphi_2. \quad (5)$$

The operator $\tilde{D} := (\partial_x^{-1}\partial_y + \partial_y^{-1}\partial_x)^{-1}$ is well-defined [13, (6)], so that u_1, u_2 can be inserted into (3). Traveling wave solutions

$$V(x, y, t) = \psi(z), \quad z = x + ky - vt \quad (6)$$

imply $\partial_x^{-1} = k\partial_y^{-1}$ and thus lead to $\varphi \equiv \text{const.} = C_0 + iC_1$. Hence, (3) can be written as

$$-v\psi_z = \frac{1-3k^2}{4}\psi_{zzz} + 6\frac{1-3k^2}{k^2+1}\psi\psi_z + 3\psi_z(C_0 + C_1k). \quad (7)$$

Following an approach outlined previously [7, 8, 14] it seems useful to find elliptic (traveling wave) solutions of the form ($p = 2$ follows from balancing the linear term of highest order with the nonlinear term in (7))

$$\psi(z) = \sum_{j=0}^{p=2} a_j f(z)^j \tag{8}$$

with [15]

$$\left(\frac{df(z)}{dz}\right)^2 = \alpha f^4 + 4\beta f^3 + 6\gamma f^2 + 4\delta f + \epsilon \equiv R(f). \tag{9}$$

The coefficients $a_0, a_1, a_2, \alpha, \beta, \gamma, \delta, \epsilon$ are assumed to be real but otherwise either arbitrary or interrelated.

Inserting (8) into (7) and using (9) we obtain a system of algebraic equations that can be reduced to yield the nontrivial solutions

$$\begin{aligned} \alpha = 0, \quad \beta = -\frac{2a_1}{1+k^2}, \quad \gamma = -\frac{4a_0}{1+k^2} + \frac{2F}{3(3k^2-1)}, \quad \delta, \epsilon \text{ arbitrary,} \\ \text{subject to } a_2 = 0, \quad 3k^2 - 1 \neq 0, \end{aligned} \tag{10}$$

$$\begin{aligned} \alpha = -\frac{2a_2}{1+k^2}, \quad \beta = -\frac{a_1}{1+k^2}, \quad \gamma = \frac{F}{6(3k^2-1)} - \frac{a_1^2 + 4a_0a_2}{4a_2(1+k^2)}, \\ \delta = \frac{1}{8a_2^2} \left(\frac{a_1^3 - 12a_0a_1a_2}{1+k^2} + \frac{2a_1a_2F}{3k^2-1} \right), \quad \epsilon \text{ arbitrary,} \\ \text{subject to } a_2 \neq 0, \quad 3k^2 - 1 \neq 0 \end{aligned} \tag{11}$$

with $F = v + 3C_0 + 3kC_1$.

Thus, the coefficients of the polynomial $R(f)$ are (partly) determined leading to solutions $f(z)$ of (9). As is well known [15, pp. 4–16], [16, p. 454] $f(z)$ can be expressed in terms of Weierstrass' elliptic function $\wp(z; g_2, g_3)$ according to

$$f(z) = f_0 + \frac{R'(f_0)}{4 \left[\wp(z; g_2, g_3) - \frac{1}{24} R''(f_0) \right]}, \tag{12}$$

where the primes denote differentiation with respect to f and f_0 is a simple root of $R(f)$.

The invariants g_2, g_3 of $\wp(z; g_2, g_3)$ and the discriminant $\Delta = g_2^3 - 27g_3^2$ are related to the coefficients of $R(f)$ [17, p. 44]. They are suitable to classify the behaviour of $f(z)$ and to discriminate between periodic and solitary wave like solutions [8].

Solitary wave like solutions are determined by (cf. (12) and Ref. [18, pp. 651–652])

$$f(z) = f_0 + \frac{R'(f_0)}{4 \left[e_1 - \frac{R''(f_0)}{24} + 3e_1 \operatorname{csch}^2(\sqrt{3e_1}z) \right]}, \quad \Delta = 0, \quad g_3 < 0, \tag{13}$$

where $e_1 = \frac{1}{2} \sqrt[3]{|g_3|}$ in (13).

In general, $f(z)$ (according to (12)) is neither real nor bounded. Conditions for real and bounded solutions $f(z)$ can be obtained by considering the phase diagram of $R(f)$ [19, p. 15]. They are denoted as “phase diagram conditions” (PDC) in the following. An example of a phase diagram analysis is given in [14].

2.2. Periodic Solutions

At first the coefficients according to (10) are considered. For simplicity we assume $\epsilon = 0$, so that $f_0 = 0$ is a simple root of (9). The solution (12) can be evaluated to yield

$$V(x, y, t) = a_0 + a_1 \frac{3(1+k^2)(1-3k^2)\delta}{(1+k^2)F + 6a_0(1-3k^2) + 3(1+k^2)(1-3k^2)\wp(x+ky-vt; g_2, g_3)} \tag{14}$$

with g_2, g_3 according to (10) and [8].

Evaluating (12) with coefficients according to (11) (with $\epsilon = 0$ for simplicity) in the same manner we obtain periodic solutions depending on a_0 , a_1 and a_2 .

2.3. Solitary Wave like Solutions

To find the subset of solitary wave like solutions of the NV equation according to (10), (13) the discriminant Δ must vanish. This is given if $\delta = 0$ or $\delta = -\frac{(6a_0(1-3k^2) + (1+k^2)F)^2}{8a_1(1-3k^2)^2(1+k^2)}$.

For $g_3 < 0$ we obtain solitary wave like solutions and here the PDC is fulfilled automatically for $g_3 < 0$.

If $\delta = 0$, $\epsilon = 0$, $f_0 = \frac{6a_0(1-3k^2) + (1+k^2)F}{2a_1(3k^2-1)}$, we obtain (cf. (8), (13))

$$V(x, y, t) = a_0 + \frac{6a_0(1-3k^2) + (1+k^2)F}{2(3k^2-1)} \operatorname{sech}^2 \left[\sqrt{-\frac{6a_0}{1+k^2} + \frac{F}{3k^2-1}}(x + ky - vt) \right]. \quad (15)$$

If $\delta = -\frac{(6a_0(1-3k^2) + (1+k^2)F)^2}{8a_1(1-3k^2)^2(1+k^2)}$, $\epsilon = 0$, $f_0 = 0$, (8) reads

$$V(x, y, t) = a_0 + \frac{6a_0(1-3k^2) + (1+k^2)F}{4(3k^2-1)} \tanh^2 \left[\sqrt{\frac{F}{2(1-3k^2)} + \frac{3a_0}{1+k^2}}(x + ky - vt) \right]. \quad (16)$$

Subject to (10) (15), (16) represent general physical traveling solitary wave solutions of the NV equation for $\epsilon = 0$. While periodic solutions depend on a_0 and a_1 , solitary solutions only depend on a_0 .

Solitary wave like solutions according to (11) can be obtained by an analogous procedure.

3. Superposition Solutions

Khare and Sukhatme proposed a superposition principle for nonlinear wave and evolution equations (NL-WEES) [9]. They have shown that suitable linear combinations of periodic traveling-wave solutions expressed by Jacobian elliptic functions lead to new solutions of the nonlinear equation in question. Combining the approach above with this superposition principle we have evaluated the following start solutions for superposition [20]

$$f(z) = \begin{cases} -\frac{3\gamma + \sqrt{9\gamma^2 - 16\beta\delta}}{4\beta} \operatorname{dn}^2 \left(\frac{1}{2} \sqrt{3\gamma + \sqrt{9\gamma^2 - 16\beta\delta}} z, \frac{2\sqrt{9\gamma^2 - 16\beta\delta}}{3\gamma + \sqrt{9\gamma^2 - 16\beta\delta}} \right), & \beta\delta > 0, \gamma > 0, \\ \frac{4\delta}{-3\gamma + \sqrt{9\gamma^2 - 16\beta\delta}} \operatorname{sn}^2 \left(\frac{1}{2} \sqrt{-3\gamma + \sqrt{9\gamma^2 - 16\beta\delta}} z, \frac{3\gamma + \sqrt{9\gamma^2 - 16\beta\delta}}{3\gamma - \sqrt{9\gamma^2 - 16\beta\delta}} \right), & \beta\delta > 0, \gamma < 0, \\ -\frac{3\gamma + \sqrt{9\gamma^2 - 16\beta\delta}}{4\beta} \operatorname{cn}^2 \left(\frac{(9\gamma^2 - 16\beta\delta)^{\frac{1}{4}}}{\sqrt{2}} z, \frac{3\gamma + \sqrt{9\gamma^2 - 16\beta\delta}}{2\sqrt{9\gamma^2 - 16\beta\delta}} \right), & \beta\delta < 0. \end{cases} \quad (17)$$

In (10) we choose $\epsilon = 0$ for simplicity and thus, we obtain start solutions for superposition according to (17). As an example we consider solutions of the form dn^2 for $p = 3$, further results for cn^2 , sn^2 and according to (11) can be obtained in the same manner.

According to (8), (10) the start solution for superposition reads

$$V(x, y, t) = a_0 + a_1 A \operatorname{dn}^2(\mu(x + ky - vt), m), \quad (18)$$

with A , μ , m according to (17), so that the superposition ansatz can be written as

$$\tilde{V}(x, y, t) = a_0 + a_1 A \sum_{i=1}^3 \operatorname{dn}^2 \left[\mu(x + ky - v_3 t) + \frac{2(i-1)K(m)}{3}, m \right]. \quad (19)$$

Inserting $\tilde{V}(x, y, t)$ (denoting $d_i = \operatorname{dn} \left(\mu(x + ky - v_3 t) + \frac{2(i-1)K(m)}{3}, m \right)$) into (7) ($v \rightarrow v_3$) and using well known relations for c_i^2 and s_i^2 [22, p. 16] leads to

$$6Aa_1\mu m(1-3k^2) \left(\mu^2 - \frac{2Aa_1}{1+k^2} \right) \sum_{i=1}^3 c_i d_i^3 s_i - \frac{12A^2 a_1^2 m \mu (1-3k^2)}{1+k^2} \sum_{i=1}^3 d_i^2 \sum_{j \neq i}^3 c_j d_j s_j \quad (20)$$

$$- 2Aa_1\mu m \left(\frac{6a_0(1-3k^2)}{1+k^2} + 3(C_0 + C_1 k) + (2-m)(1-3k^2)\mu^2 + v_3 \right) \sum_{i=1}^3 c_i d_i s_i = 0.$$

Remarkably, $\mu^2 - \frac{2Aa_1}{1+k^2}$ vanishes automatically [20, (13)]. By use of [23], (21) reads

$$\begin{aligned}
 & -2Aa_1\mu m \left(\frac{6a_0(1-3k^2)}{1+k^2} + 3(C_0 + C_1k) + (2-m)(1-3k^2)\mu^2 + v_3 \right) \sum_{i=1}^3 c_i d_i s_i \\
 & -2Aa_1\mu m \left(-\frac{12Aa_1(1-3k^2)(m-1+q^2)}{(1+k^2)(1-q^2)} \right) \sum_{i=1}^3 c_i d_i s_i = 0.
 \end{aligned} \tag{21}$$

Thus, the speed v_3 in the superposition solution (19) is given by

$$v_3 = \frac{6a_0(3k^2-1)}{1+k^2} - 3(C_0 + C_1k) + (2-m)(3k^2-1)\mu^2 + \frac{12Aa_1(3k^2-1)(m-1+q^2)}{(1+k^2)(q^2-1)}. \tag{22}$$

The start solution V and the superposition solution \tilde{V} are shown in Fig. 1.

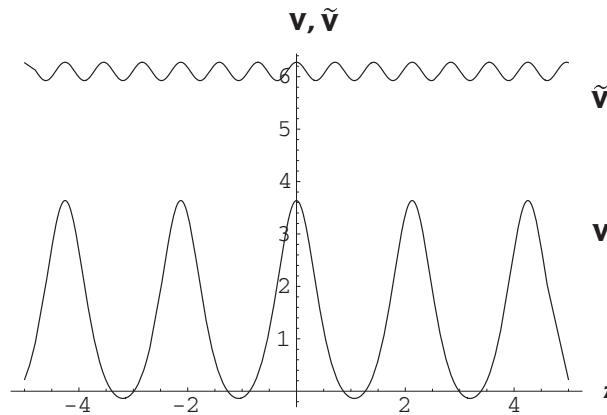


Figure 1: V and \tilde{V} (cf. (18), (19)) for $c = -1$, $k = 1$, $a_0 = -1$, $a_1 = -1$, $C_0 = 1$, $C_1 = 1$, $\delta = 4$ (therefore: $v_3 = -8.66008$).

4. Conclusion

For the NV equation we have shown that a rather broad set of traveling wave solutions according to (6), (8) and subject to the nonlinear ordinary differential equation (9) can be obtained. Periodic and solitary wave solutions can be presented in compact form in terms of Weierstrass' elliptic function and its limiting cases ($\Delta = 0$, $g_3 \leq 0$), respectively. The phase diagram conditions (PDC) yield constraints for real and bounded solutions. Finally, it is shown that application of the Khare-Sukhatme superposition principle yields new periodic (real, bounded) solutions of the NV equation.

Acknowledgment

One of us (J. N.) gratefully acknowledges support by the German Science Foundation (DFG) (Graduate College 695 "Nonlinearities of optical materials").

REFERENCES

1. Novikov, S. P. and A. P. Veselov, "Two-dimensional Schrödinger operator: Inverse scattering transform and evolutionary equations," *Physica D*, Vol. 18, 267–273, 1986.
2. Bogdanov, L. V., "Veselov-Novikov equation as a natural two-dimensional generalization of the Korteweg-de Vries equation," *Theor. Math. Phys.*, Vol. 70, 309, 1987.
3. Tagami, Y., "Soliton-like solutions to a (2+1)-dimensional generalization of the KdV equation," *Phys. Lett. A*, Vol. 141, 116–120, 1989.
4. Cheng, Y., "Integrable systems associated with the Schrödinger spectral problem in the plane," *J. Math. Phys.*, Vol. 32, 157–162, 1990.

5. Taimanov, I. A., "Modified Novikov-Veselov equation and differential geometry of surfaces," arXiv: dg-ga/9511005 v5 20 Nov. 1995.
6. Ferapontov, E. V., "Stationary Veselov-Novikov equation and isothermally asymptotic surfaces in projective differential geometry," *Differential Geometry and its Applications*, Vol. 11, 117–128, 1999.
7. Schürmann, H. W. and V. S. Serov, "Traveling wave solutions of a generalized modified Kadomtsev-Petviashvili equation," *J. Math. Phys.*, Vol. 45, 2181–2187, 2004.
8. Schürmann, H. W. and V. S. Serov, "Weierstrass' solutions to certain nonlinear wave and evolution equations," *Proc. Progress in Electromagnetics Research Symposium*, Pisa, 651–654, 2004.
9. Cooper, F., et al., "Periodic solutions to nonlinear equations obtained by linear superposition," *J. Phys. A: Math. Gen.*, Vol. 35, 10085–10100, 2002.
10. Khare, A. and U. Sukhatme, "Cyclic identities involving Jacobi elliptic functions," *J. Math. Phys.*, Vol. 43, 3798–3806, 2002.
11. Khare, A. and A. Lakshminarayan, "Cyclic identities for Jacobi elliptic and related functions," *J. Math. Phys.*, Vol. 44, 1822–1841, 2003.
12. Khare, A. and U. Sukhatme, "Linear superposition in nonlinear equations," *Phys. Rev. Lett.*, Vol. 88, 244101-1 – 244101-4, 2002.
13. Veselov, A. P. and S. P. Novikov, "Finite-gap two-dimensional potential Schrödinger operators. Explicit formulas and evolution equations," *Dokl. Akad. Nauk SSSR*, Vol. 279, 20–24, 1984.
14. Schürmann, H. W., "Traveling-wave solutions of the cubic-quintic nonlinear Schrödinger equation," *Phys. Rev. E*, Vol. 54, 4312–4320, 1996.
15. Weierstrass, K., *Mathematische Werke V*, Johnson, New York, 1915.
16. Whittaker, E. T. and G. N. Watson, *A Course of Modern Analysis*, Cambridge University Press, Cambridge, 1927.
17. Chandrasekharan, K., *Elliptic Functions*, Springer, Berlin, 1985.
18. Abramowitz, M. and I. A. Stegun, *Handbook of Mathematical Functions*, 9th ed., Dover, New York, 1972.
19. Drazin, P. G., *Solitons*, Cambridge University Press, Cambridge, 1983.
20. Schürmann, H. W., et al., "Superposition in nonlinear wave and evolution equations," arXiv: nlin.SI/05-08015 v2 22 Aug. 2005.
21. Bronstein, I. N., et al., *Taschenbuch der Mathematik*, 5th ed., Verlag Harri Deutsch, Thun und Frankfurt am Main, 2000.
22. Milne-Thomson, L. M., *Jacobian Elliptic Function Tables*, Dover Publications, New York, 1950.
23. cf. Ref. [12], Eq. (11); cf. Ref. [9], Eqs. (7), (8).

Source Representations of the Debye Potentials in Spherical Coordinates

M. J. Lahart

U.S. Army Research Laboratory, USA

In a widely cited paper [1], Bouwkamp and Casimir derived the relationship between the Debye scalar potentials and their charge and current sources. They did this by computing the electric and magnetic fields associated with each of the potentials and using Maxwell's equations to compute the charge and current sources. Their derivation specified that the scalar potentials could only be defined outside a sphere that contained all of the charge and current sources. Nisbet [2] challenged the need for this restriction and claimed that the Debye potentials could be defined everywhere, including regions that contained charge and current sources.

This presentation examines the need to define the Debye potentials only in regions where the charge and current sources are zero. Some possible definitions of scalar potentials in terms of magnetic and electric vector potentials will be examined. It will be shown that, to be consistent with Maxwell's equations, some definitions require that the scalar potentials obey the wave equation, while others require that only the components of the gradients of the potentials in two orthogonal directions obey the wave equation. In spherical coordinate systems, only the latter type of definition is possible; potentials that obey the wave equation cannot be defined, but potentials whose gradient components in the θ and ϕ directions can be. By expressing the Debye potentials in terms of the magnetic and electric vector potentials and examining the consistency of the expressions with Maxwell's equations, it will be shown that one of the potentials can be defined in regions that contain charges and currents and the other cannot.

For comparison, it will be shown that scalar potentials that obey the wave equation can be defined in rectangular coordinates. Because of this, a pair of potentials can be defined in regions where charge and current sources are present. An example will be given by expressing fields in a waveguide in terms of scalar potentials and their charge and current sources.

REFERENCES

1. Bouwkamp, C. J. and H. B. G. Casimir, "On multipole expansions in the theory of electromagnetic radiation," *Physica (Utrecht)*, Vol. 20, 539–554, 1954.
2. Nisbet, A., "Source representations for Debye's electromagnetic potentials," *Physica(Utrecht)*, Vol. 21, 799–802, 1955.

On the Stability of the Electromagnetic Field in Inhomogeneous Anisotropic Media With Dispersion

N. V. Budko

Delft University of Technology, The Netherlands

A. B. Samokhin

Moscow University of Radioengineering and Electronics, Russia

From the electromagnetic point of view various meta-materials, optical crystals, geophysical formations, ice, magnetized plasma, etc., can be described as inhomogeneous anisotropic media with dispersion. The interaction of the electromagnetic field with such media can be studied by different analytical and numerical methods. When a three-dimensional object is of finite extent and is situated in free space, then the method of choice is the Volume Integral Equation (VIE) method, sometimes referred to as the Domain Integral Equation method (mathematical literature) and the Discrete Dipole Approximation (physics).

In contrast to the one- and two-dimensional cases, where existence of the solution to the scattering problem is a trivial question, in the three-dimensional case solution exists under certain conditions related to the physical properties of the medium in question. Note that the sufficient uniqueness conditions are basically the same for all cases. Previously we have shown that the singular integral operator of the VIE has an essential continuous spectrum, which is given explicitly in terms of the constitutive parameters of an inhomogeneous object. Now we shall extend this result to anisotropic media with dispersion. We shall also prove that in the quasi-static case the discrete eigenvalues are contained within the complex envelope of the continuous spectrum.

For anisotropic media with dispersion, especially for magnetized plasma, the question of considerable interest is the stability of such a medium. Within the commonly adopted approach, based on the differential form of the Maxwell's equations and Lorentz or Vlasov's equations of motion, very little can be said about the stability of *inhomogeneous* objects of finite extent, whereas the VIE formulation is perfectly suited for this task. Instead of analyzing the stability of the medium itself we propose to analyze the stability of the electromagnetic field in a given medium. Due to self-consistency of the problem the two approaches are in fact identical. Thus, we shall discuss the stability of the field in several practical cases ranging from optical crystals to plasma.

Scattering of Electromagnetic Waves by Inhomogeneous Dielectric Gratings Loaded with Perfectly Conducting Strips

T. Yamasaki, T. Ujiie, and T. Hinata
Nihon University, Japan

The scattering and guiding problems of inhomogeneous dielectric gratings have been of considerable interest such as optical fiber gratings, photonic bandgap crystals, frequency selective devices, and other applications by the development of manufacturing technology of optical devices. Recently, many analytical and numerical methods which are applicable to the arbitrarily dielectric gratings have been proposed. However, most theoretical and numerical studies have considered the periodic structures in which the material forming grating was either metallic or dielectric.

In this paper, we proposed a new method for the scattering of electromagnetic waves by inhomogeneous dielectric gratings loaded with perfectly conducting strips using the combination of improved Fourier series expansion method and point matching method.

In the inhomogeneous dielectric region $S_2(0 < x < d)$, the permittivity profile $\varepsilon_2(x, z)$ is generally not separable with respect to the x and z variables. Main process of our methods are as follows: (1) The inhomogeneous layer is approximated by an assembly of M stratified layers of modulated index profile with step size $d_\Delta (\triangleq d/M)$. (2) Taking each layer as a modulated dielectric grating, the electromagnetic fields are expanded appropriately by a finite Fourier series. (3) In the perfectly conducting strip and gap regions at C and \bar{C} for the boundary, the electromagnetic fields are matched on both sides using point matching method (3) Finally, all stratified layers include the metallic regions are matched using appropriate boundary conditions to get the inhomogeneous dielectric gratings loaded with perfectly conducting strips.

Numerical results are given for the transmitted scattered characteristics for the case of incident angle both TM and TE waves.

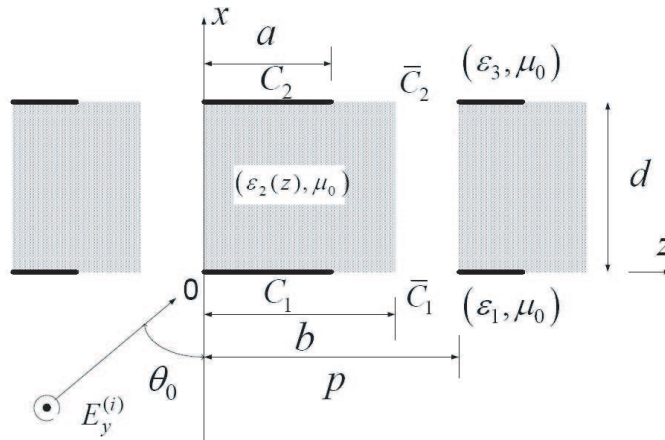


Figure 1: Structure of inhomogeneous dielectric gratings loaded with perfectly conducting strips.

Effects of the Resonant Scattering of Intensive Fields by Weakly Nonlinear Dielectric Layer

V. V. Yatsyk

Nat. Acad. of Sci. of Ukraine, Ukraine

Abstract—The transverse inhomogeneous, isotropic, nonmagnetic, linearly polarized, weakly nonlinear (a Kerr-like dielectric nonlinearity) dielectric layer is considered. The results of a numerical analysis of the diffraction problem of a plane wave on the weakly nonlinear object with positive and negative value of the susceptibility are shown. The effects: non-uniform shift of resonant frequency of the diffraction characteristics of a weakly nonlinear dielectric layer; itself the channeling of a field; increase of the angle of the transparency of the nonlinear layer when growth of intensity of the field (at positive value of the susceptibility); de-channeling of a field (at negative value of the susceptibility) are found out.

1. The Nonlinear Problem

Let the time dependence be $\exp(-i\omega t)$ and $\vec{E}(\vec{r})$, $\vec{H}(\vec{r})$ complex amplitudes of an electromagnetic field. We consider a nonmagnetic, isotropic, transverse inhomogeneous $\varepsilon^{(L)}(z) = 1 + 4\pi\chi_{xx}^{(1)}(z)$, linearly polarized $\vec{E} = (E_x, 0, 0)$, $\vec{H} = (0, H_y, H_z)$ (E -polarized) and Kerr-like weakly nonlinearity $P_x^{(NL)} = \frac{3}{4}\chi_{xxxx}^{(3)}|E_x|^2 E_x$, $\max_{|z| \leq 2\pi\delta} (|\alpha| \cdot |E_x|^2) \ll \max_{|z| \leq 2\pi\delta} |\varepsilon^{(L)}(z)|$ (where $\vec{P}^{(NL)} = (P_x^{(NL)}, 0, 0)$ — vector of polarization, $\alpha = 3\pi\chi_{xxxx}^{(3)}$, $\chi_{xx}^{(1)}$ and $\chi_{xxxx}^{(3)}$ is the components of susceptibility tensor) dielectric layer (Fig. 1), [1, 2].

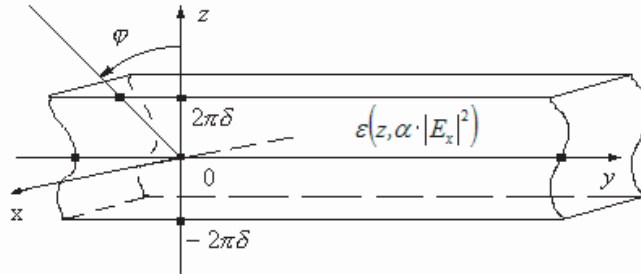


Figure 1: Weakly nonlinear dielectric layer: $\max_{|z| \leq 2\pi\delta} (|\alpha| \cdot |E_x|^2) \ll \max_{|z| \leq 2\pi\delta} |\varepsilon^{(L)}(z)|$.

The complete diffraction field $E_x(y, z) = E_x^{inc}(y, z) + E_x^{scat}(y, z)$ of a plane wave $E_x^{inc}(y, z) = a^{inc} \exp[i(\phi y - \Gamma \cdot (z - 2\pi\delta))]$, $z > 2\pi\delta$ on the nonlinear dielectric layer (Fig. 1) satisfies such conditions of the problem:

$$\nabla^2 \cdot \vec{E} + \frac{\omega^2}{c^2} \cdot \varepsilon^{(L)}(z) \cdot \vec{E} + \frac{4\pi\omega^2}{c^2} \cdot \vec{P}^{(NL)} \equiv \left(\nabla^2 + \kappa^2 \cdot \varepsilon(z, \alpha \cdot |E_x|^2) \right) \cdot E_x(y, z) = 0, \quad (1)$$

the generalized boundary conditions:

$$\begin{aligned} E_{tg} \text{ and } H_{tg} \text{ are continuous at discontinuities } \varepsilon(z, \alpha \cdot |E_x|^2); \\ E_x(y, z) = U(z) \cdot \exp(i\phi y), \text{ the condition of spatial quasihomogeneity along } y; \end{aligned} \quad (2)$$

the condition of the radiation for scattered field:

$$E_x^{scat}(y, z) = \left\{ \begin{array}{l} a^{scat} \\ b^{scat} \end{array} \right\} \cdot e^{i(\phi y \pm \Gamma \cdot (z \mp 2\pi\delta))}, \quad z \begin{array}{l} > \\ < \end{array} \pm 2\pi\delta \quad (3)$$

Here: $\varepsilon(z, \alpha \cdot |E_x|^2) = \begin{cases} 1, & |z| > 2\pi\delta \\ \varepsilon^{(L)}(z) + \alpha \cdot |E_x|^2, & |z| \leq 2\pi\delta \end{cases}$; $\nabla^2 = \frac{\partial^2}{\partial y^2} + \frac{\partial^2}{\partial z^2}$; $\alpha = 3\pi\chi_{xxxx}^{(3)}$; $\Gamma = (\kappa^2 - \phi^2)^{1/2}$; $\phi \equiv \kappa \cdot \sin(\varphi)$; $|\varphi| < \pi/2$ (see Fig. 1); $\kappa = \omega/c \equiv 2\pi/\lambda$; $c = (\varepsilon_0 \mu_0)^{-1/2}$, ε_0 , μ_0 and λ length of the wave are the parameters of environment.

In this case the required solution of the problem (1)–(3) has the form:

$$E_x(y, z) = U(z) \cdot e^{i\phi y} = \begin{cases} a^{inc} \cdot e^{i(\phi y - \Gamma \cdot (z - 2\pi\delta))} + a^{scat} \cdot e^{i(\phi y + \Gamma \cdot (z - 2\pi\delta))}, & z > 2\pi\delta, \\ U^{scat}(z) \cdot e^{i\phi y}, & |z| \leq 2\pi\delta, \\ b^{scat} \cdot e^{i(\phi y - \Gamma \cdot (z + 2\pi\delta))}, & z < -2\pi\delta. \end{cases} \quad (4)$$

Here $U(-2\pi\delta) = b^{scat}$, $U(2\pi\delta) = a^{inc} + a^{scat}$.

The nonlinear problem (1)–(3) is reduced to finding the solutions $U(z) \in L_2([-2\pi\delta, 2\pi\delta])$ (see (4)) of the inhomogeneous nonlinear integrated equation of the second kind [3, 4]:

$$U(z) + \frac{i\kappa^2}{2\Gamma} \int_{-2\pi\delta}^{2\pi\delta} \exp(i\Gamma \cdot |z - z_0|) \left[1 - (\varepsilon^{(L)}(z_0) + \alpha |U(z_0)|^2) \right] U(z_0) dz_0 = U^{inc}(z), \quad |z| \leq 2\pi\delta, \quad (5)$$

where $U^{inc}(z) = a^{inc} \exp[-i\Gamma \cdot (z - 2\pi\delta)]$.

The integrated equation (5) with application of the quadrature method and use (4) is reduced to system of the nonlinear equations of the second kind [4].

2. Susceptibility and Effects Resonant Scattering of the Intensive Fields

2.1. Intensity and Resonant Frequency

The effect of non-uniform shift of resonant frequency of the diffraction characteristics of nonlinear dielectric layer is found out at increase of intensity of inciting field [4, 5] (see Fig. 2(a), at positive value of the susceptibility $\alpha = 0.01$, and also Fig. 2(b), at negative value of the susceptibility $\alpha = -0.01$). Growth of intensity of

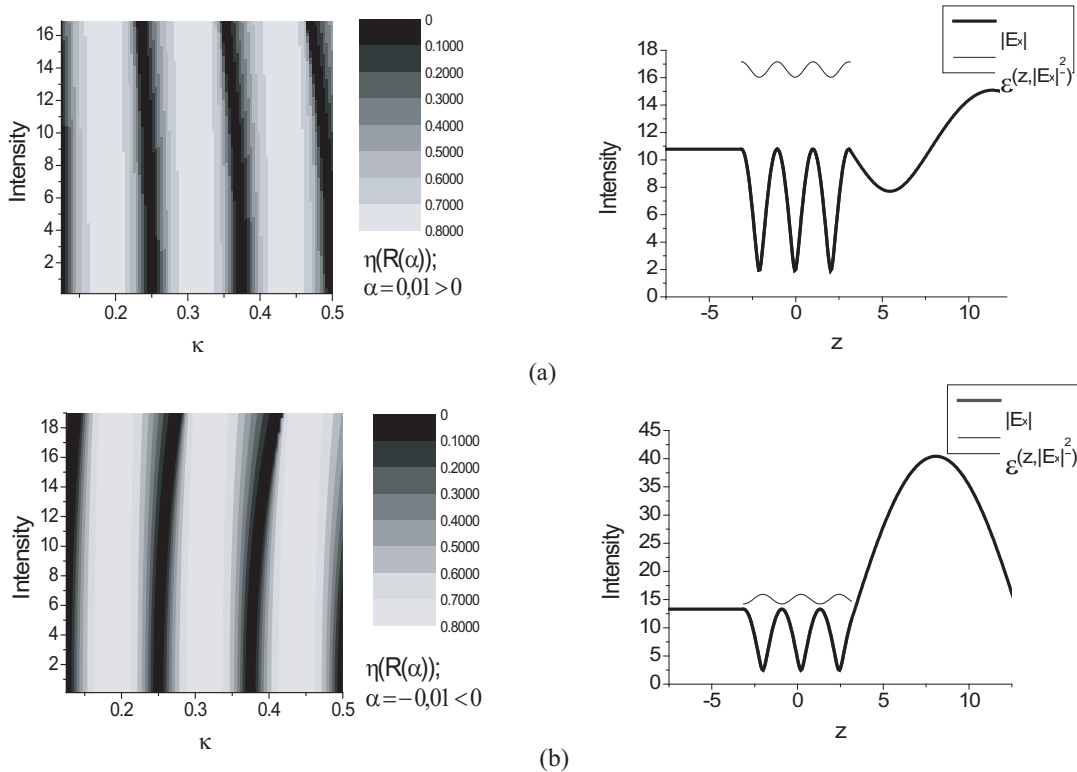


Figure 2: Parameters of structure: $\delta = 0.5$; $\varphi = 45^\circ$; $\kappa = 0.375$; $\varepsilon^{(L)} = 16$. (a) $|I| = |a^{inc}| = 11.4$; $\alpha = 0.01$, (b) $|I| = |a^{inc}| = 22.4$; $\alpha = -0.01$.

the inciting field $|I| = |a^{inc}|$ results in change of the share of the reflected wave $\eta(R(\alpha)) = |R(\alpha)|^2 / |I|^2$ (here $|R(\alpha)| \equiv |a^{scat}(\alpha)|$, $|T(\alpha)| \equiv |b^{scat}(\alpha)|$, $|I|^2 = |T(\alpha)|^2 + |R(\alpha)|^2$): reduction of value of resonant frequency with increase and reduction of a steepness of the diffraction characteristics before and after resonant frequency

(Fig. 2(a), at $\alpha > 0$); increase of value of resonant frequency with reduction and increase of a steepness of the diffraction characteristics before and after resonant frequency (Fig. 2(b), at $\alpha < 0$).

2.2. Intensity and Angle

The effects: itself the channeling of a field — increase of the angle of the transparency of the nonlinear layer ($\alpha \neq 0$) when growth of intensity of the field (Fig. 3(a), at positive value of the susceptibility, $\alpha > 0$); de-channeling of a field (Fig. 3(b), at negative value of the susceptibility, $\alpha < 0$) are found out, [4, 5].

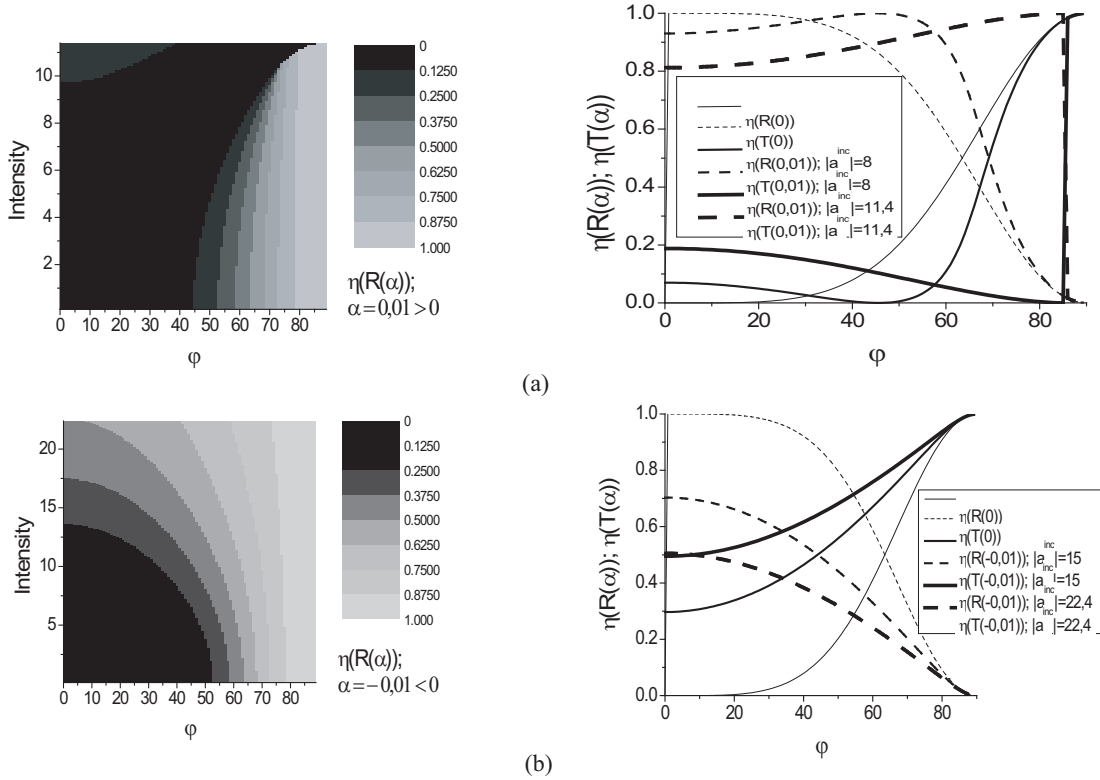


Figure 3: Parameters of structure: $\delta = 0.5$; $\kappa = 0.375$; $\varepsilon^{(L)} = 16$; for linear layer with $\alpha \equiv 0$ and for nonlinear layer: a with $\alpha = 0.01$; b with $\alpha = -0.01$.

The increase of the angle of a transparency with growth of intensity at positive value of the susceptibility $\alpha = 0.01$ is easy for tracking on Fig. 3(a): $|a^{inc}| = 8$, $\varphi \approx 46^\circ$ and $|a^{inc}| = 11.4$, $\varphi \approx 85^\circ$.

Weak nonlinearity of a dielectric layer $\varepsilon(z, \alpha \cdot |E_x|^2) \equiv \varepsilon(z, \alpha \cdot |U|^2)$,

$$\max_{|z| \leq 2\pi\delta} (|\alpha| \cdot |E_x|^2) \ll \max_{|z| \leq 2\pi\delta} |\varepsilon^{(L)}(z)|, \quad (6)$$

i. e., the small nonlinear additive $\alpha |U(z)|^2$ to a linear part $\varepsilon^{(L)}(z)$ of the dielectric permeability, caused by intensity $|U^{inc}|$ of a field of excitation of nonlinear object, results in essential changes diffraction characteristics. Exceeding some critical threshold of intensity the statement (6) loses force, computing process is broken. For example, diffraction characteristics reach critical values with growth of intensity of field, see lines for $\alpha > 0$ on Fig. 3(a): point of a transparency $\varphi = \varphi^*(|a^{inc}|)$, where $\eta(R)|_{\varphi=\varphi^*(|a^{inc}|)} = 0$ and $\eta(T)|_{\varphi=\varphi^*(|a^{inc}|)} = 1$, here $\varphi^*(|a^{inc}|)$ defined from: $\frac{d\eta(R)}{d\varphi}|_{\varphi=\varphi^*(|a^{inc}|)} = \frac{d\eta(T)}{d\varphi}|_{\varphi=\varphi^*(|a^{inc}|)} = 0$, weakly nonlinear layer aspires to limiting value $\varphi^*(|a^{inc}|) \rightarrow 90^\circ$ at $|a^{inc}| \rightarrow \max\{|a^{inc}|\} = 11.5$. The analysis of results for $\alpha < 0$ on Fig. 3(b) shows, that limiting critical values $\eta(R)|_{\varphi=\varphi^*(|a^{inc}|) \equiv 0^\circ} \rightarrow 0.5$ and $\eta(T)|_{\varphi=\varphi^*(|a^{inc}|) \equiv 0^\circ} \rightarrow 0.5$ at $|a^{inc}| \rightarrow \max\{|a^{inc}|\} = 22.4$ lay on curves of translucent $\eta(R) = \eta(T) = 0.5$ weakly nonlinear structure. It allows to estimate numerically size of required intensity of a field of excitation

$$\max_{|z| \leq 2\pi\delta} (|\alpha| \cdot |U(z)|^2) \leq \max_{|z| \leq 2\pi\delta} (|\alpha| \cdot |U^{inc}(z)|^2) < C \cdot \max_{|z| \leq 2\pi\delta} |\varepsilon^{(L)}(z)| \quad (7)$$

to make an estimation weakly sizes C , at which (6) does not lose force with growth of intensity of a field of excitation of a nonlinear layer.

For example, see Fig. 3(a), (where: $\varepsilon^{(L)}(z) = 16$, $\alpha = 0.01$), convergence of iterative process is broken when $|U^{inc}| > 11.5$. From (7) it is received: $C = 0.083$. Hence, weak nonlinearity proves at intensity not surpassing $|U^{inc}| = 11.5$ and variations of small nonlinearity layer: $\max_{|z| \leq 2\pi\delta} (|\alpha| \cdot |U(z)|^2) < 1.328$.

These effects (see sections 2.1 and 2.2) are connected to resonant properties of a nonlinear dielectric layer and caused by increase at positive value of the susceptibility or reduction at negative value of the susceptibility of a variation of dielectric permeability of a layer (its nonlinear components) when increase of intensity of a field of excitation of researched nonlinear object.

3. Conclusion

The principal fields where the results of our numerical analysis are applicable are as follows: the investigation of wave self-influence processes; the analysis of amplitude-phase dispersion of eigen oscillation-wave fields in the nonlinear objects, see [6]; extending the description of evolutionary processes near to critical points of the amplitude-phase dispersion of nonlinear structure; new tools for energy selecting, transmitting, and remembering devices; etc.

REFERENCES

1. Akhmediev, N. N. and A. Ankiewicz, *Solitons*, Fizmatlit, Moscow, 2003.
2. Yariv, A. and P. Yeh, *Optical Waves in Crystals*, Mir, Moscow, 1987.
3. Shestopalov, V. P. and Y. K. Sirenko, *Dynamic Theory of Gratings*, Naukova Dumka, Kiev, 1989.
4. Yatsyk, V. V., "The numerical simulations and resonant scattering of intensive electromagnetic fields of waves by dielectric layer with Kerr-like nonlinearity," *E-print: Computational Physics*, <http://arxiv.org/pdf/physics/0412109>, No. 12, 1–11, 2004.
5. Yatsyk, V. V., "Effects of resonant scattering of the intensive fields by nonlinear layer," 2005 Workshop on Fundamental Physics of Ferroelectrics (Ferro2005), <http://www.mri.psu.edu/conferences/ferro2005>, Williamsburg, Virginia, USA, February 6–9, 83–84, 2005.
6. Yatsyk, V. V., "Diffraction problem and amplitudes-phases dispersion of eigen fields of a nonlinear dielectric layer," *E-print: Computational Physics, Optics*, <http://arxiv.org/pdf/physics/0503089>, No. 3, 1–13, 2005.

Theoretical Analysis of Convergence of Rao-Wilton-Glisson Method and Subhierarchical Parallel Algorithm for Solving Electric Field Integral Equation

Y. G. Smirnov

Penza State University, Russia

We consider three-dimensional problem of the electromagnetic wave diffraction by bounded and perfectly conducting screen of arbitrary shape in free space. The problem is reduced to the electric field integral equation (EFIE) [1]. We use very popular Rao-Wilton-Glisson (RWG) method for solving this problem. We have proved theorem of convergence in special Sobolev spaces and obtained estimation of the rate of convergence for RWG method.

The main difficulties in RWG method are very large time of calculations of matrix elements with sufficiently high accuracy and occurrence of large and dense matrices in systems of linear algebraic equations obtained after discretization of the problem.

If one uses RWG method for the problem discretization, the matrix elements may be calculated independently. A natural way to calculate the matrix elements is utilization of parallel computations using supercomputers or clusters. Note in addition that the structure of matrices is not arbitrary: in the diffraction problems. We have the so-called structured matrices with $O(n)$ different elements, where n denotes the matrix dimension.

We have created and elaborated efficient solvers for several types of diffraction problems on the basis of subhierarchical algorithms of parallel computations [2].

*This study is carried out under the support of the Russian Foundation for Basic Research, grant no 03-07-90274.

REFERENCES

1. Ilyinsky, A. S. and Y. G. Smirnov, *Electromagnetic Wave Diffraction by Conducting Screens*, VSP Int. Science Publishers, Utrecht, the Netherlands, 1998.
2. Medvedik, M. Y. and Y. G. Smirnov, "Subhierarchical parallel computational algorithm and convergence of Galerkin Method in electromagnetic diffraction problem on plane screen," *Izvestiya Vyzov, Povolzsky Region, Estestvennye Nauki*, ü 5, 3–19, 2004 (in Russian).